CrystEngComm

PAPER

View Article Online
View Journal

Cite this: DOI: 10.1039/d6ce00043f

Correlating thermal history to structural integrity and cycling stability in NMC 111 cathodes

Jeffrey S. Ovens,[a] Rex Chen,[a] Yingzi Feng,[b] Majid Talebiesfandarani,[b] Stephen A. Campbell[b] and Byron D. Gates *[a]

Thermal treatment is critical for determining the structure and stability of layered cathode materials, which in turn affect the performance of lithium-ion batteries. This study systematically investigated the thermal evolution of NMC 111 cathode materials synthesized from prelithiated precursors. Thermogravimetric analysis and variable-temperature X-ray diffraction were employed to monitor phase transitions and mass loss over a wide temperature range. The material transformed from a calcite-type carbonate to rock salt and subsequently to the layered NMC 111 structure, with crystallization largely complete near 800 °C. Cation mixing can begin around 500 °C but remains reversible upon cooling if the sample is heated to 800 °C or lower. In contrast, prolonged thermal soaking at high temperatures (≥900 °C) causes irreversible structural degradation, including the emergence of Li-deficient spinel phases attributed to lithium volatilization. An optimal soak temperature of 800 °C was identified, balancing high crystallinity with minimal irreversible cation mixing. Material synthesized at 800 °C also exhibited greater cycling stability than materials processed at higher temperatures. A dwell time of ~6 hours is sufficient to produce high-quality NMC 111 materials. Balancing dwell time and upper-temperature thresholds is essential during synthesis. These findings offer practical guidance for optimizing thermal treatments used to manufacture layered cathodes for lithium-ion batteries.

Received 16th January 2026,
Accepted 5th May 2026

DOI: 10.1039/d6ce00043f

rsc.li/crystengcomm

Introduction

The global transition to renewable energy technologies is driving demand for advanced energy storage systems. In particular, lithium-ion batteries (LIBs) are now widely used in electric vehicles, portable electronics, and grid-scale storage applications where a long cycle life, high energy density, and thermal stability are essential.[1–3] The cathode material is one of the most critical and cost-intensive components of LIBs.[4] The cathode plays a central role in determining the overall energy density, stability, and performance of this type of battery. Among various cathode chemistries for LIBs, lithium nickel manganese cobalt oxide with an equimolar composition of transition metals (*i.e.*, NMC 111) is a prototypical layered oxide material,[5–8] offering a well-balanced combination of electrochemical performance and structural stability. The NMC 111 cathode material can also serve as a model system for studying its structural evolution and optimizing the synthesis of Ni-based layered oxides. Its relatively simple composition and stable behaviour make it an ideal material for developing design rules that can be applied to higher nickel-content materials such as $LiNi_{0.6}Mn_{0.2}Co_{0.2}O_2$ (NMC 622), $LiNi_{0.8}Mn_{0.1}Co_{0.1}O_2$ (NMC 811), and lithium nickel cobalt aluminum oxide (NCA), which are more prone to cation mixing and phase degradation under thermal stresses.[9–11]

Despite its advantages, the electrochemical properties of NMC 111 are highly sensitive to synthesis conditions, particularly thermal treatment protocols.[5,12] The layered structure of NMC materials, characterized by alternating layers of lithium and transition metals, requires precise thermal management to achieve optimal crystallinity and cation ordering.[13] Insufficient temperatures may lead to incomplete phase formation and the presence of residual carbonates or other impurities from the precursor materials. In contrast, elevated temperatures can cause lithium volatilization, irreversible cation mixing, and the formation of undesired phases such as spinel or rock-salt structures. Thermal processing also introduces significant challenges for large-scale manufacturing, where the trade-off between energy efficiency and material quality becomes increasingly important.[14] High-temperature synthesis enhances crystallinity, but increases energy consumption and exacerbates oxygen loss, leading to cation mixing and structural degradation.[15] Lower-temperature thermal treatments, while more energy-efficient, may fail to

[a] *Department of Chemistry, Simon Fraser University, 8888 University Drive, Burnaby, BC V5A 1S6, Canada. E-mail: bgates@sfu.ca*
[b] *Nano One Materials Corporation, 8575 Government St, Burnaby, BC, V3N 4V1, Canada*

eliminate structural inhomogeneities and/or to achieve complete crystallization of the cathode material. Additionally, internal temperatures within secondary particles can result in non-uniform formation of the desired phase and inconsistent material properties.[14] These issues are further complicated by the difficulty of translating lab-scale conditions to industrial-scale processes. Therefore, precisely defining an optimal thermal window is essential to achieve the desired phase purity and crystallinity, to minimize structural defects, ensure consistency across scales, and enable cost-effective, high-performance cathode production.

Although several studies have investigated the thermal behaviour of NMC materials, systematic insights into the combined effects of soak temperature and dwell time on phase evolution and cation ordering remain limited. For example, studies have systematically investigated the impact of calcination temperatures on the structural, morphological, and electrochemical properties of Ni-rich $LiNi_{0.76}Mn_{0.14}Co_{0.10}O_2$ (NMC 76) cathode materials.[16] The authors identified an optimal temperature range (*i.e.*, 750 to 775 °C) that minimized cation mixing and microcracking in the cathode materials while enhancing their cycling stability and rate capability. Another study investigated the impact of excess lithium content, the synthesis method, and sintering temperature on the quality of NMC 111 cathode materials.[17] Their findings demonstrated that higher sintering temperatures and the use of more homogenous precursors – particularly those prepared by spray-drying – promoted the formation of a single-phase product, reduced cation mixing, and improved the electrochemical performance of this cathode material. These works highlighted the importance of fine-tuning synthesis and thermal treatment protocols to maintain phase integrity and optimize cathode performance; however, they did not systematically isolate or optimize the soak temperature and dwell time as independent variables. Building on these foundational studies, the work presented herein uses NMC 111 as a model system to comprehensively explore the effects of thermal treatment—specifically, soak temperature and dwell time—on crystallinity, cation mixing, and phase purity. While some prior studies have employed *in situ* techniques, relatively few have tracked structural transformations in real time across a wide temperature range using complementary tools. To address this need, this study integrates thermogravimetric analysis (TGA) with variable temperature X-ray diffraction (VT-XRD) to monitor the thermal evolution of carbonate-derived NMC 111 precursors with high resolution and fidelity.

This study systematically investigates the effects of thermal treatment conditions—specifically calcination temperature, dwell time, and thermal cycling—on the structural evolution and phase purity of NMC 111 synthesized from prelithiated carbonate precursors. A combination of TGA and VT-XRD is employed to monitor phase transitions from carbonate intermediates to rock-salt-type structures and the final layered phase. Cation ordering is quantitatively assessed using the I_{003}/I_{104} intensity ratio (R_1) from XRD measurements,[18,19] which indicates that temperatures above 800 °C result in irreversible structural degradation due to lithium volatilization and the formation of spinel-type impurities. These temperature-dependent structural findings were subsequently correlated with electrochemical performance to establish a thermally optimal processing window that enhances the product crystallinity while minimizing irreversible cation mixing and phase instability. The findings provide valuable design rules for synthesizing high-quality NMC 111 materials and offer broader insights into thermal-treatment strategies for preparing advanced layered oxide cathodes.

Experimental methods

Synthesis of NMC 111 powders

Prelithiated NMC 111 precursors were provided by Nano One Materials Corp. and were used as received. The active cathode materials were prepared by heating the respective NMC 111 precursor in air at either 800 °C for 10 h or 900 °C for 5 h with a ramp rate of 5 °C min^{-1}. The synthesized powders were collected after cooling to room temperature.

Variable temperature X-ray diffraction (VT-XRD) measurements

All VT-XRD data were collected in air on a Bruker D8 Advance diffractometer equipped with a Cu Kα (λ = 1.54184 Å) sealed-tube source, a LynxEye high-speed detector and an Anton Paar HTK 1200 N heating chamber. A 1 mm divergence slit and 2.5° Soller slit were in place. The scanning rate was either 1.2 s per step or 1.6 s per step with a step size of ~0.02°. The heating rate when changing the sample temperature was 0.5 °C s^{-1}, with a stabilization time of 60 s upon reaching the set point temperature.

Thermogravimetric analysis (TGA)

A Perkin Elmer TGA 8000 with an Autosampler under the control of Pyris software was used to collect TGA data. A continuous flow of air was used to purge the sample chamber, maintaining an oxidizing atmosphere during these analyses. For each sample, a method file was created to define the heating profile. Samples were heated to their maximum temperature at a rate of 10 °C min^{-1}. Measurements were performed by TGA as single replicates to establish the broad temperature regimes for thermal decomposition of the prelithiated NMC 111 precursor, as well as for lithium acetate and the relevant metal carbonates. Isothermal holds were included when necessary to mimic the synthesis conditions. The empty platinum sample basket was first tared, then filled with 5 to 10 mg of sample powder and weighed again before starting the run. After each run, the baskets were cleaned in an ultrasonic bath and baked at 200 °C to remove any residual moisture or contamination before reuse.

Flame atomic absorption spectroscopy (FAAS)

Before performing elemental analysis by FAAS, the samples were digested using aqua regia (4 : 1, v/v mixture of 37% HCl

and 70% HNO_3). *Caution: these reagents are corrosive, and appropriate precautions should be taken when handling them.* Approximately 100 mg of cathode material was weighed by difference and transferred to a 125 mL Erlenmeyer flask containing a stir bar. Aqua regia (30 mL) was added, and the mixture was stirred overnight in a fume hood. The resulting solution was diluted 100-fold with 2% HNO_3 to match the matrix used in the standard solutions.

Calibration standards were prepared using a two-step dilution process from 1000 ppm commercial stock solutions. First, intermediate 100 ppm standards for each element (*i.e.*, Li, Ni, Mn, and Co) were created by diluting 10 mL of the 1000 ppm stock solution into a 100 mL volumetric flask, using 2% HNO_3 as the diluent. From these 100 ppm solutions, a series of multi-element working standards was prepared at concentrations of 1, 2, and 5 ppm. For NMC 111 samples, the standards were prepared by combining the following volumes of each 100 ppm solution: (i) 1 ppm standard: 1 mL Li, 3 mL Ni, 1 mL Mn, and 1 mL Co; (ii) 2 ppm standard: 2 mL Li, 6 mL Ni, 2 mL Mn, and 2 mL Co; and (iii) 5 ppm standard: 5 mL Li, 15 mL Ni, 5 mL Mn, and 5 mL Co.

A 100 g L^{-1} KCl solution was added to suppress ionization interference during lithium analysis. The Perkin Elmer PinAAcle 500 was calibrated using this series of standard solutions and Syngistix software. For each element, a dedicated hollow-cathode lamp was installed and allowed to warm up for at least 15 min to ensure signal stability. The operating software automatically selected the lamp, and the procedure did not require manual alignment by the operator. An air-acetylene flame was used for all measurements, with the burner head position optimized for each analysis based on the element of interest. The primary analytical wavelengths used were (i) 670.78 nm for Li, (ii) 232.0 nm for Ni, (iii) 279.48 nm for Mn, and (iv) 240.73 nm for Co, with a constant slit width of 0.2 nm for all analyses. After baseline correction and analysis of a blank solution, standard curves were generated and used to quantify elemental concentrations in the digested samples. All samples were extensively mixed before analysis, and the capillary intake tube leading to the nebulizer was rinsed with deionized water and 2% HNO_3 between each measurement to prevent cross-contamination.

Evaluation of electrochemical stability

Electrochemical analyses of the NMC 111 materials were performed using CR2032 coin cells. A cathode slurry of the NMC 111 powders was prepared by mixing the cathode particles with conductive carbon black (C65, Gelon LIB Group) and a polyvinylidene fluoride binder (PVDF, Solvay, Solef 51300/1001 high viscosity grade) using *N*-methyl-2-pyrrolidinone as the solvent (NMP, Gelon LIB Group, electronic grade 99.9%). The final weight ratio of the solid contents was 90% NMC 111 cathode material, 7% carbon black, and 3% PVDF. The resulting ink was cast on a 16 μm-thick graphite-coated aluminum foil current collector using a doctor blade to form a thin electrode with an NMC loading of 5 mg cm^{-2}. The electrodes were dried for 24 h at 80 °C under vacuum (≥685 Torr). These dried, coated electrodes were calendared to a thickness of ~35 μm to achieve an approximate electrode density of 3 g cm^{-3}.

A series of 1.5 cm^2 disks was cut from the electrodes and transferred into an argon-filled glovebox for assembly into the coin cells. Lithium foil disks, 340 μm thick, were used as counter and reference electrodes. The electrolyte used was a 1 M $LiPF_6$ solution in a mixture of ethylene carbonate (EC), ethyl methyl carbonate (EMC), and dimethyl carbonate (DMC) containing a 1% vinylene carbonate (VC) electrolyte additive. The polypropylene separators in the coin cells were 19 mm in diameter and 25 μm in thickness. An electric crimper was used to assemble and seal the cells. The cells were conditioned for 10 cycles at a rate of C/10 before being cycled at 1C over a voltage range of 2.5 V to 4.2 V (*vs.* Li/Li^+) for 200 cycles at 25 °C.

Results and discussion

To systematically evaluate the influence of thermal treatment parameters on the structural development and stability of NMC 111, the following sections are organized around key experimental findings that align with each phase of material transformation. First, TGA and VT-XRD are used to determine the thermal decomposition and phase evolution pathways of the carbonate-derived precursor, thereby identifying the critical temperature ranges for structural transitions. Second, the effects of prolonged soaking at fixed temperatures are investigated using time-resolved XRD to track the development of crystallinity and cation ordering, with special emphasis on the I_{003}/I_{104} (R_1) ratio as an indicator of Li/Ni mixing. Third, thermal cycling experiments assess the reversibility of structural changes and delineate the thermal threshold beyond which cation disorder becomes irreversible. Finally, the presence of impurity phases is examined *via* XRD of thermally treated samples, providing evidence for lithium volatilization and spinel formation under harsh processing conditions. These results enable a correlative interpretation of thermal history, crystallographic features, and implications for optimizing synthesis parameters in layered oxide cathode materials.

Investigating the thermal transformation pathway of the NMC 111 precursor

A fundamental understanding of the thermal transformation pathway from precursor to the layered NMC 111 phase is essential for optimizing the synthesis conditions and controlling the quality of this cathode material. The thermal decomposition of carbonate-based precursors is known to involve multiple overlapping mass-loss and phase-transition events, which can influence crystallization behaviour and lithium distribution within the final structure.[20,21] These analyses use a combination of TGA and VT-XRD to track the mass-loss profile and corresponding structural evolution of a

prelithiated precursor containing $Ni_{1/3}Mn_{1/3}Co_{1/3}CO_3$ and lithium acetate (LiOAc) over a broad temperature range. These analyses accurately identify the key temperature intervals associated with dehydration, carbonate decomposition, and phase evolution. For example, these studies provide critical insights into the formation and stability of intermediate and final crystalline phases as a function of temperature.

Data from the TGA analyses of the $Ni_{1/3}Mn_{1/3}Co_{1/3}CO_3$/LiOAc precursor shows three distinct regions of mass loss (Fig. S1): (i) 30 to 160 °C; (ii) 200 to 280 °C; and (iii) 280 to 400 °C. The lowest temperature range corresponds to the evaporation of any residual moisture in the sample and/or hydration of the precursor species. The other two temperature ranges correspond to the decomposition and volatilization of CO_3^{2-} and OAc^- from the precursors. These processes result in the release of CO, CO_2 and H_2O vapour from the sample. At higher temperatures (>450 °C), a continuous, slow mass loss continues at a decreasing rate until it approaches a stable mass at approximately 900 °C. This behaviour is distinct from the sharper, discrete transitions observed at lower temperatures and is not attributable to further decomposition of carbonate or acetate species, which are largely complete by ~400 °C. Instead, this slow mass loss is consistent with a combination of processes, including the release of oxygen from nascent transition metal oxides and the volatilization of lithium-containing species—particularly Li_2O or LiOH formed from the decomposition of residual LiOAc. Lithium compounds, especially Li_2CO_3 or Li_2O, can become volatile or react with ambient moisture and/or CO_2 at elevated temperatures.[22] These additional transformations can result in a steady mass loss in the TGA profile. This region's absence of distinct inflection points or sharp peaks further supports a diffusion-limited, kinetically sluggish process such as lithium evaporation[15,23] or structure reconstruction.[24,25] Furthermore, no appreciable mass loss or gain is observed during cooling.

To facilitate a more in-depth analysis of the processes taking place at temperatures above 200 °C, a series of TGA analyses were also performed for $NiCO_3$, $MnCO_3$, $CoCO_3$ and $LiOAc{\cdot}2H_2O$ (Fig. S2 to S5). The thermal decomposition of each transition metal carbonate involves a multi-step process. The initial mass loss corresponds to the removal of water. The subsequent thermal decomposition of the carbonate species results in the conversion of the metal to its oxide, accompanied by the release of CO_2.[26–28] The onset temperature of decomposition varies between the different carbonate species. The $NiCO_3$ decomposes at a lower temperature than the $MnCO_3$ and $CoCO_3$. Additionally, $MnCO_3$ and $CoCO_3$ exhibit a mass loss between 850 and 900 °C, possibly indicating volatilization of reaction products[28] or further oxidation of the transition metal.[29] It appears that while this process is irreversible for $MnCO_3$, it is reversed upon cooling down the $CoCO_3$ sample. In addition to the initial mass loss attributed to a dehydration of the precursors, $LiOAc{\cdot}2H_2O$ exhibits two primary mass losses between 350 and 425 °C and from 725 to 850 °C. These thermal transformations of the sample likely correspond to the thermal decomposition of the acetate group and the subsequent thermal breakdown of lithium carbonate, respectively.[30] A gradual, continuous mass loss is observed above 850 °C, reaching a maximum loss at 1000 °C in the TGA measurements. This final transformation is possibly due to the volatilization of lithium-containing species, such as Li_2O, or the slow decomposition of residual lithium salts.[31,32]

It is notable that when heating the $Ni_{1/3}Mn_{1/3}Co_{1/3}CO_3$/LiOAc precursor, its mass loss profile differs from those observed for the separate thermal treatment of each of the transition metal carbonates. The TGA response of the $Ni_{1/3}Mn_{1/3}Co_{1/3}CO_3$/LiOAc precursor was not a simple combination of the profiles observed for each feedstock used to create the $Ni_{1/3}Mn_{1/3}Co_{1/3}CO_3$/LiOAc precursor. The thermal degradation profile of the precursor most closely resembled that of $NiCO_3$. These observations collectively suggest that the $Ni_{1/3}Mn_{1/3}Co_{1/3}CO_3$/LiOAc precursor is not a physical mixture of $NiCO_3$, $MnCO_3$, and $CoCO_3$, but is rather a chemically integrated material. The unique thermal profile supports the interpretation that the $Ni_{1/3}Mn_{1/3}Co_{1/3}CO_3$/LiOAc precursor is a single-phase solid solution of the transition metals, formed before calcination. While the transition metal carbonates serve as precursors in the synthesis, the final mixed $Ni_{1/3}Mn_{1/3}Co_{1/3}CO_3$/LiOAc precursor product represents a distinct, compositionally homogeneous phase.

Performing a series of survey scans by VT-XRD while incrementally ramping the temperature from 30 to 1000 °C (Fig. 1a–d) reveals several structural transformations that occur during the thermal treatment of the $Ni_{1/3}Mn_{1/3}Co_{1/3}CO_3$/LiOAc precursor. Due to the small crystal domain size inherent to the thermal transformations of the prelithiated material, which also indicates its partial amorphous character, the initial XRD peaks are very broad at the onset of the thermal treatment (*i.e.*, low temperatures). There is, however, sufficient definition in these initial XRD patterns to determine the crystallographic phases present therein. For example, the $Ni_{1/3}Mn_{1/3}Co_{1/3}CO_3$ species in the precursor mixture forms a calcite-type structure with alternating layers of transition metals and carbonate. This phase is captured in the low-temperature patterns (yellow) in Fig. 1a and illustrated graphically in Fig. 1d (left-most, yellow box). Upon heating the sample to 200 °C, a complete structural transformation occurs, with the sample transitioning to a rock-salt structure. This transformation also corresponds to the decomposition of carbonate anions, the release of CO_2, and the oxidation of Mn^{2+} and Co^{2+} cations to Mn^{4+} and Co^{3+}, respectively. This transformation is captured in Fig. 1c, wherein VT-XRD data were collected at 10 °C increments between 130 and 190 °C. These results show that this transformation occurs within a relatively narrow range of 150 to 170 °C. This reaction occurs at a lower temperature in VT-XRD than observed by TGA, which may be due to the slower ramp rate used in VT-XRD. The VT-XRD required longer data collection times at each temperature step. These measurements resulted in longer dwell times at each temperature for VT-XRD than for TGA. The TGA data are also likely complicated by the concurrent decomposition of LiOAc, which is not observable in

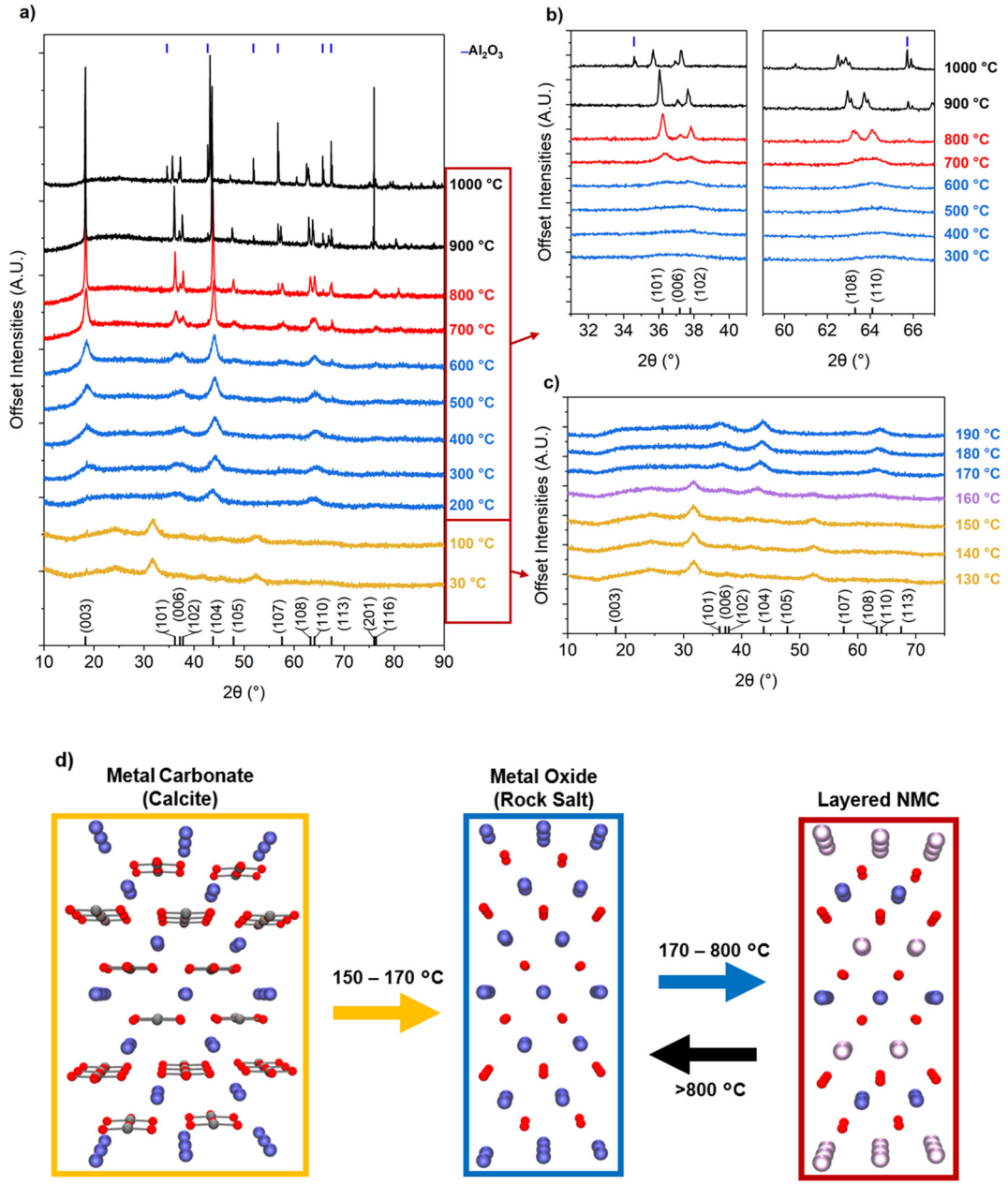

Fig. 1 VT-XRD analysis of the thermal evolution of a prelithiated $Ni_{1/3}Mn_{1/3}Co_{1/3}CO_3$/LiOAc precursor from 30 to 1000 °C. (a) Full-range diffraction patterns showing phase transitions during heating. (b) Expanded views of key 2θ regions highlighting the development and collapse of layered reflections. (c) High-resolution scans (130 to 190 °C) showing the sharp transition from a calcite-type to rock-salt phase. (d) Schematic of structural evolution: calcite-like NMC 111 precursor → rock-salt → layered NMC 111. Al_2O_3 marked with blue bars.

the XRD patterns due to its amorphous nature and the relatively weak diffraction from lithium in the lithiated species.[33]

As the newly formed rock-salt phase is heated further, Li^+ gradually diffuses into the structure. The onset of this process begins around 300 °C, segregating the transition metals and Li^+ cations into separate layers and eventually forming the layered NMC 111 structure. This structural change is evident from the gradual formation of the (003) peak at ~18.5° (2θ) and the splitting of the rock-salt (111) peak at ~36° (2θ) into the (102), (006) and (101) peaks associated with the layered R-3m phase.[34] Upon reaching 800 °C, the XRD pattern of the heated sample shows sharp, well-defined reflections consistent with the formation of fully crystallized, layered NMC 111. The structure resulting from this transformation is depicted in the central image of Fig. 1d (blue box), which shows the formation of alternating Li and transition metal layers. However, above 800 °C, these three peaks associated with the R-3m phase begin to recombine, suggesting a gradual transition back to a rock-salt phase. This transformation may occur through the loss of Li^+ and/or by mixing the layers of Li^+ and transition metal cations. This structural degradation is captured in the VT-

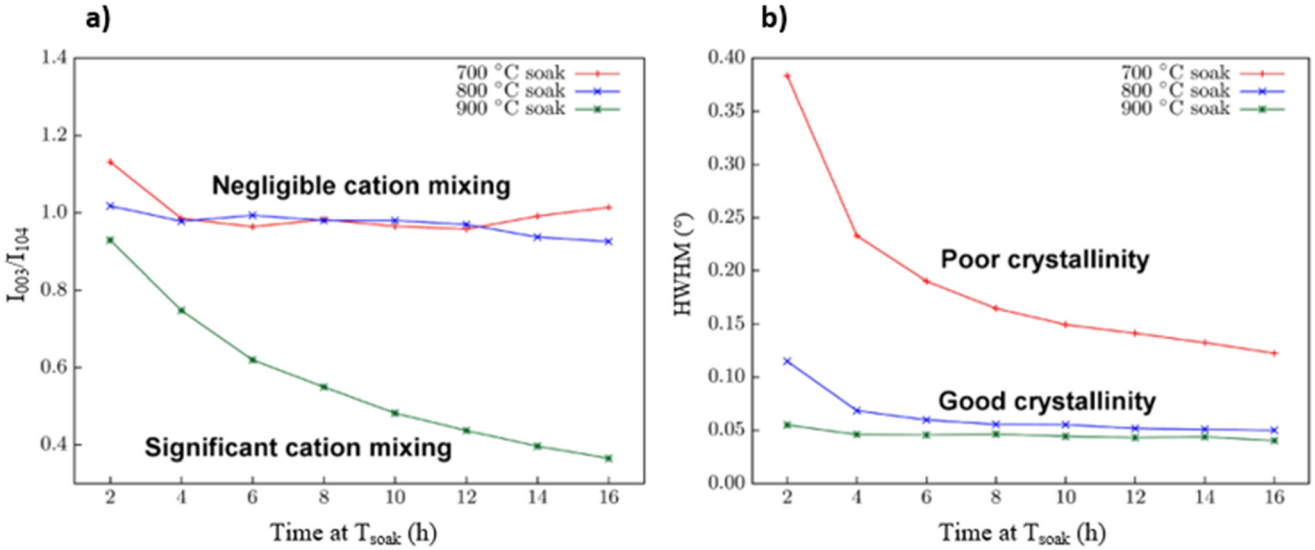

Fig. 2 Evolution of structural quality in NMC 111 during prolonged thermal soaking at 700 °C, 800 °C, and 900 °C. (a) Cation ordering tracked *via* the intensity ratio $R_1 = I_{003}/I_{104}$; lower values indicate increased cation mixing. (b) Sample crystallinity as assessed by the half-width at half-maximum (HWHM) of the (104) peak; narrower peaks indicate improved crystallinity.

XRD analyses performed from 900 to 1000 °C, as depicted in Fig. 1a and b and summarized in Fig. 1d (right-hand, red box).

Exploring the effects of isothermal soaking on structural ordering

The evolution of cation ordering is of particular interest to the transformations that occur during the thermal treatment of the NMC precursor. This transformation occurs within the reaction mixture during the high-temperature soak phase, which is the period during which the material is maintained at a constant elevated temperature following the initial heating ramp. To investigate this transition to cation ordering in more detail, the precursor mixture was heated to the maximum temperature (*i.e.*, 700, 800, or 900 °C) and held at that temperature for 16 h. During this extended soak phase, powder XRD data were collected every 2 h to monitor the degree of cation mixing and the crystallinity of the *in situ* synthesized material.

Cation mixing is characterized by using the R_1 value, which equals the ratio of the integrated intensities of the (003) and (104) planes of crystalline NMC. This method of characterizing cation mixing is effective since the (003) planes coincide with distinct layers of ordered cations. Without cation mixing, these planes correspond to alternating layers of transition metal cations and Li^+ cations. In a system where Li^+ and transition metal cations are perfectly mixed, these two layers become identical, leading to a systematic absence (*i.e.*, zero intensity) for the (003) planes in favour of the (006) planes. A partially mixed system results in a partial absence or a decrease in the I_{003} intensity. Cation mixing does not affect I_{104} in NMC as the (104) planes pass through both the transition metal and Li^+ cation sites. The (104) planes are, therefore, used as an internal standard, enabling a direct comparison of the ratio to the I_{003} intensity (*i.e.*, $R_1 = I_{003}/I_{104}$) between samples without interference from slight variations arising from instrumental or sample preparation effects.[18,19] Generally, for NMC materials, R_1 values less than 1.2 indicate an undesirable degree of cation mixing, which is known to degrade electrochemical performance, whereas R_1 values greater than 1.2 indicate minimal cation mixing.[18,35]

Fig. 2a shows the evolution of cation mixing as tracked by the intensity ratio $R_1 = I_{003}/I_{104}$ over the 16 h soak period. Separate samples were used for each set-point temperature. Fig. 2b tracks the change in crystallinity for each sample, evaluated from the (104) peak half-width at half-maximum (HWHM) for the samples held at soak temperatures of 700, 800, and 900 °C. The HWHM measures the width of a diffraction peak at half its maximum intensity; a smaller HWHM, corresponding to a narrower, sharper peak, indicates a higher degree of crystallinity and larger crystallite domains within the heated sample. Narrower peaks generally indicate a higher degree of crystallinity in a sample than those samples with broader peaks. However, peak broadening is influenced by the instrument, crystallite (domain) size, and internal microstrain, which contribute independently to the peak width.[36,37] The influences of instrumental broadening were not subtracted from the peak width measurements, as the relative trends over time remain robust for comparing the results of the isothermal soaks. Furthermore, while XRD peak widths are a convolution of crystallite size and microstrain (which can, in principle, be decoupled using the Williamson–Hall approach),[38] domain size is expected to be the dominant contributor to the broadening observed in these samples. Therefore, the trend toward narrower peaks during soaking reflects an increase in crystallite domain size

rather than a relief in microstrain. The minimal change in HWHM at 800 °C and 900 °C over time suggests that crystallite coarsening and strain relief are mostly complete early in the soak period. However, only the 800 °C condition achieves this without compromising cation ordering.

The R_1 values in Fig. 2a for samples treated at soak temperatures of 700 and 800 °C show negligible changes with soak time (*i.e.*, these samples remain relatively constant in terms of cation mixing, as assessed by R_1). In contrast, when the precursor material is soaked at 900 °C, the R_1 value rapidly declines over time. This result indicates the presence of a thermal barrier to cation mixing, which is breached when the sample is soaked at a temperature between 800 and 900 °C. Below this temperature threshold, no significant cation rearrangements occur. In contrast, a change in the crystallinity of the sample, as quantified by the HWHM, is nearly instantaneous when treated at 900 °C (Fig. 2b). A similar change in crystallinity also occurs relatively rapidly when the precursor material is heated for 16 h at 800 °C. In contrast, at a soak temperature of 700 °C, the crystallinity of the sample improves only slightly over 16 h. This sample, treated at a lower temperature, does not achieve a comparable HWHM to those of samples treated at higher temperatures within a reasonable time frame.

The combined results of these two analyses can serve as a guide for selecting the appropriate thermal treatment conditions for NMC-type materials. This selection of thermal treatment conditions should identify both the maximum temperature that prevents cation mixing and the minimum temperature that promotes crystallization. It is important to acknowledge that these measurements were conducted at elevated temperatures, which can influence the VT-XRD data.[39] Thermal expansion of the crystal lattice shifts diffraction peaks to lower 2θ angles, while increased atomic thermal vibrations broaden the peaks. Although the VT-XRD experiments herein did not include an internal standard to correct for these effects, their influence on the conclusions is considered negligible. Since the R_1 value is a ratio of two peak intensities, and both peaks are subject to these thermal effects, the impact is expected to be proportional and largely cancel out, leaving the R_1 ratio as a robust indicator of cation ordering. Similarly, the HWHM are also influenced; increased atomic vibration introduces a thermal broadening component to the peaks, which is superimposed on the broadening from crystallite size and microstrain. This means that the absolute HWHM measured at elevated temperatures is likely to be larger than at room temperature. However, because the soak experiments are conducted isothermally, the observed trends in HWHM over time accurately reflect changes in the material's intrinsic crystallinity. Furthermore, the fact that the HWHM for the 800 and 900 °C samples is significantly lower than for the 700 °C sample, despite the greater thermal broadening at the higher temperature, reinforces the conclusion that thermal treatment in the range of 800 to 900 °C promotes substantially higher crystallinity.

Identifying reversible *vs.* irreversible structural degradations

The results described above demonstrate that excessively high soak temperatures can lead to undesirable attributes in thermally processed materials. It is essential to understand whether this damage is reversible or permanent. To evaluate the reversibility of these changes, synthesized NMC 111 samples were subjected to thermal cycling. Each sample was heated to a soak temperature of either 800 or 900 °C, held at this temperature for 6 h, and subsequently cooled to 30 °C. This cycle of heating, soaking, and cooling was repeated twice more, resulting in a total of three complete thermal cycles. During heating and cooling, data were acquired at 25 °C intervals over the temperature range in which the critical transformations were observed (*e.g.*, 400 to 900 °C). In contrast, data were acquired at 100 °C intervals over the temperature range that has exhibited more structural stability (*e.g.*, 30 to 400 °C). During the soak periods, diffraction patterns were collected approximately every hour to capture the time-dependent structural evolution of the sample while it was held at a constant temperature. The resulting R_1 values for each of these thermal cycles were plotted as a function of temperature, as shown in Fig. 3.

During soaking at 900 °C (Fig. 3a), the R_1 value decreases rapidly to ~0.75 over the initial 6 h of thermal soaking. During the first cooling phase, the R_1 value recovers, but only to ~1.05. This R_1 value is reached upon cooling the sample to 300 °C. Further cycles of ramping, soaking, and cooling

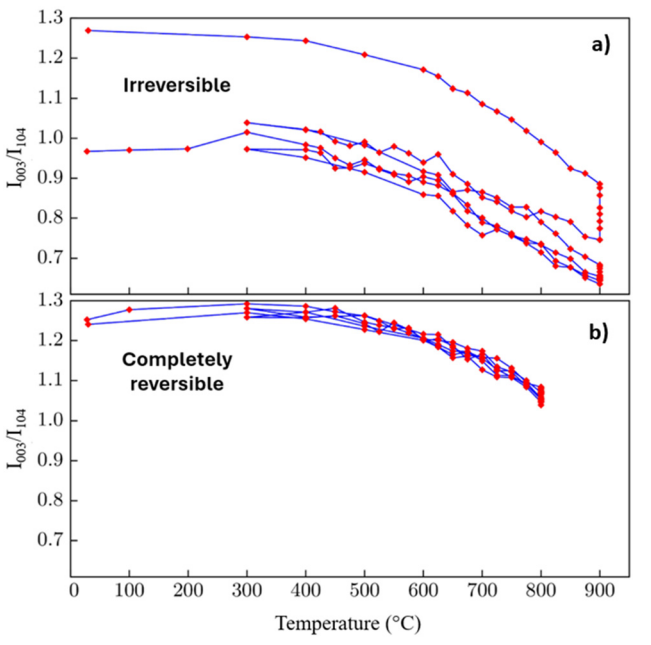

Fig. 3 Evolution of the cation ordering parameter $R_1 = I_{003}/I_{104}$ during thermal cycling of NMC 111 samples. (a) Samples cycled at 900 °C exhibit irreversible loss of cation ordering, as indicated by the progressive decline in R_1 with sequential heating cycles. (b) In contrast, samples cycled at 800 °C show fully reversible cation ordering, with R_1 values recovering upon each cooling cycle.

result in a further decline in R_1; however, this factor mostly recovers upon cooling the sample. At the end of the series of thermal cycles, the final R_1 value was ~1.0 with a 900 °C thermal soak. In contrast, setting the thermal soak to a maximum of 800 °C results in a negligible decrease in R_1 (Fig. 3b). In this case, the R_1 value completely recovers upon cooling the sample to 300 °C. In addition, any changes to the R_1 value remain reversible during the subsequent two thermal cycles that reach 800 °C. These results indicate the relative impact of thermal treatment of the prelithiated precursor on R_1, as reflected in changes in microstrain and in the observed XRD features (*e.g.*, peak broadening and changes in peak intensity), compared with those changes resulting from irreversible cation mixing.

For this set of measurements, a pre-synthesized NMC product was used to minimize dimensional and morphological changes in the precursor material during the thermal reaction to form the final NMC 111 material. The R_1 value at room temperature is ~1.3 at the start of the experiment. Upon heating the synthesized material to ~500 °C, the R_1 value begins to decrease due to the onset of cation mixing. It is crucial to recognize that the decrease observed at high temperatures is a convoluted effect and may not represent purely cation mixing. Several factors may contribute to the apparent structural changes observed during the VT-XRD experiments, including thermal expansion of the lattice, which shifts peak positions, and increased atomic vibrations (attributed to the Debye–Waller effect), which reduce peak intensities and contribute to thermal broadening.[40,41] Furthermore, small thermal gradients within the sample chamber can also influence the peak shape and position.[42] While Debye–Waller effects and increased atomic vibrations contribute to thermal broadening at elevated temperatures, the R_1 values reported herein were calculated using the ratio of integrated intensities (*i.e.*, peak areas) rather than a ratio of peak heights. Because thermal broadening conserves the total diffracted area, and since the (003) and (104) peaks remain well-resolved during the high-temperature soaks, the R_1 ratio effectively neutralizes these thermal artifacts. This makes the ratio of integrated peak area intensities a robust metric for tracking irreversible cation mixing, even in the absence of an internal standard.

There are a few noteworthy observations in these results: (i) cation mixing in NMC 111 can occur at temperatures as low as 500 °C; (ii) as long as the maximum temperature does not exceed a threshold, potential cation mixing and the impact of thermally induced microstrain only increases as a function of temperature and not as a function of dwell time at elevated temperatures; (iii) potential changes in cation mixing and thermally induced strain reverses itself upon cooling as long as this temperature threshold is not exceeded; and (iv) upon crossing a thermal barrier (*i.e.*, between 800 and 900 °C for prelithiated NMC 111), irreversible cation mixing occurs within the sample. Thus, it appears that two separate processes occur during the thermal treatment of NMC 111. Both reversible and irreversible processes are taking place within the samples. Establishing the upper thermal limit is essential to avoid irreversible cation mixing.

Irreversible processes that result in cation mixing are of great interest for NMC 111 and other layered cathode materials. These processes can degrade the performance of these materials when used as cathode materials in LIBs. Thus, select powder XRD profiles from the two thermal cycling experiments were investigated in greater detail. Fig. 4 shows the final room temperature powder XRD profiles obtained after thermal cycling of the sample to a maximum temperature of 800 °C (Fig. 4a) and 900 °C (Fig. 4b). In each plot, an inset shows a magnified view of the region around the (003) reflection. While the profile in Fig. 4a is nearly identical to that for the pristine NMC 111 material, the profile in Fig. 4b contains impurity peaks that have a significant intensity. The impurity was attributed to a Li-deficient spinel phase.[43,44] This spinel phase is depicted as LiM_2O_4 where M = $\{Ni_xMn_yCo_z\}$ and $x + y + z = 1$. As lithium is lost from the structure by high-temperature volatilization, the layered framework becomes unstable and transitions to the thermodynamically stable Li-deficient spinel phase. Prior art shows that the transformation from the layered phase proceeds *via* an intermediate, disordered rock-salt phase to the spinel phase.[45] This transformation is fundamentally driven by the irreversible loss of lithium and oxygen from the lattice. In this study, the high-temperature volatilization of lithium at 900 °C creates this critical lithium deficiency, providing the thermodynamic driving force for the layered oxide to reorganize into the more stable, albeit electrochemically inferior, spinel structure. This lithium loss is quantitatively supported by flame atomic absorption spectroscopy (FAAS) in Table S1, which confirms a reduction in the relative stoichiometry from 0.9675 at 800 °C to 0.9399 at 900 °C.

An additional thermal cycling experiment was performed using a lithium-deficient NMC 111 material. In this experiment, the sample underwent the same thermal cycle as the sample in Fig. 4a (*i.e.*, with a maximum soak temperature of 800 °C). The final powder XRD profile after thermal cycling of a material intentionally synthesized with a 15 at% Li^+ deficiency is plotted in Fig. 5. In these results, the spinel impurity peaks are also present, as observed in Fig. 4b for the sample treated with a 900 °C thermal soak. This result further suggests that Li^+ cations are lost from the sample when heated above a specific threshold temperature. This temperature is between 800 and 900 °C for the prelithiated NMC 111. This optimal temperature window for NMC 111 is notably higher than that reported for more nickel-rich NMC compositions. For instance, investigations into Ni-rich NMC 76 identified an optimal calcination temperature range of 750 to 775 °C, with temperatures ≥800 °C leading to excessive primary particle growth and poor cycling stability.[16] Similarly, studies on the direct regeneration of spent NMC 811 have used a lower processing temperature of 750 °C, which is attributed to the presence of a preformed crystalline lattice.[46] These comparisons suggest that as the nickel content of NMC materials increases, their thermal stability decreases, necessitating lower synthesis and processing temperatures to mitigate severe structural degradation and Li^+/Ni^{2+} cation

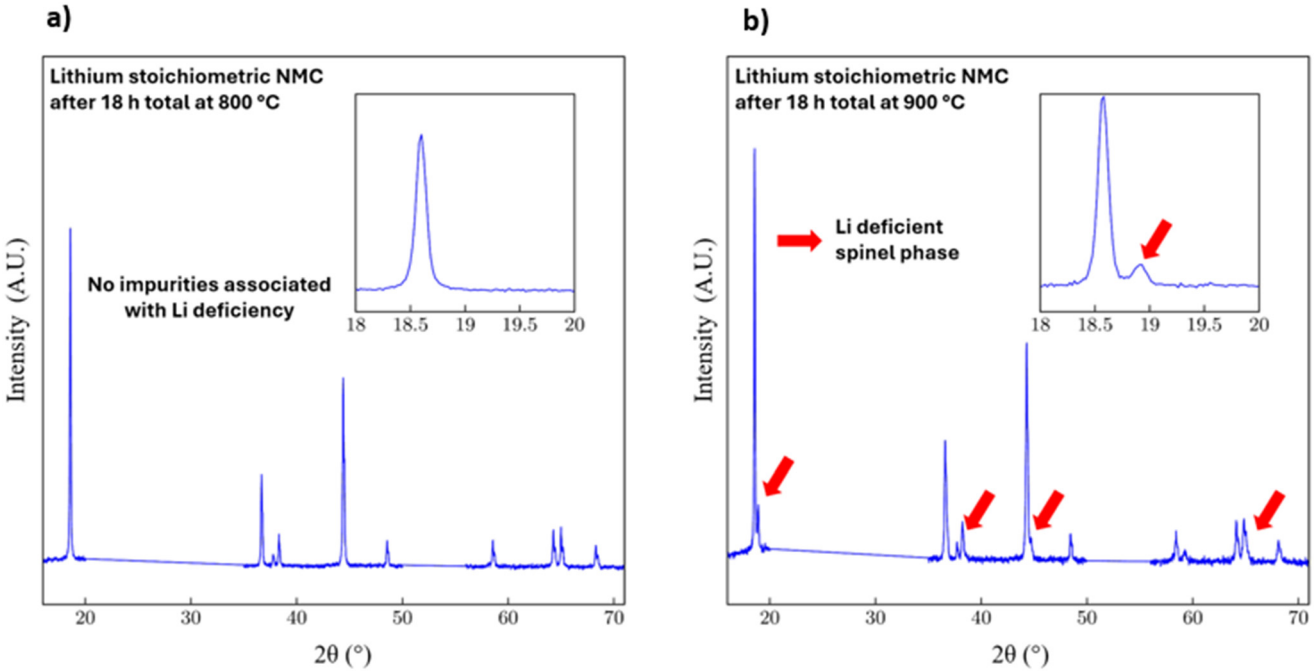

Fig. 4 Room temperature powder XRD patterns obtained for NMC 111 after thermal cycling to either (a) 800 °C or (b) 900 °C. No impurity peaks are observed for the sample cycled to 800 °C, while the sample treated at 900 °C shows reflections (red arrows) from a Li-deficient spinel phase (LiM_2O_4, M = Ni, Mn, Co). Insets highlight changes near the (003) peak, indicating the effects of irreversible cation disorder induced at higher temperatures.

mixing. The atomic voids created in the sample by processes associated with lithium removal at elevated temperatures could be partially filled with Ni^{2+} cations. This high-temperature induced loss of lithium is often attributed to the decomposition of unreacted or residual lithium precursors (*e.g.*, LiOH) into more volatile species, such as Li_2O, which can then be removed from the system during calcination.[47,48] Accordingly, once the Li^+ cations are lost from the sample, they are not reacquired during the cooling cycle. As a result, irreversible damage would occur to the sample, as observed during thermal cycling of prelithiated NMC 111.

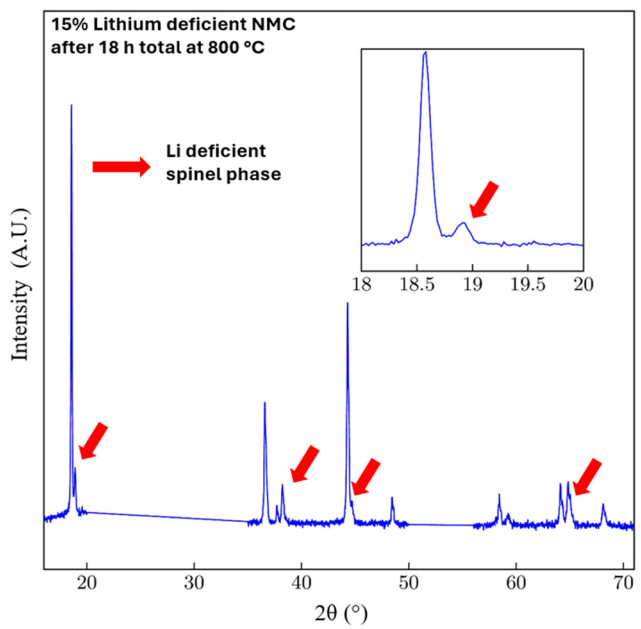

Fig. 5 Powder XRD patterns of 15% lithium-deficient NMC after 18 h at 800 °C. Reflections from a Li-deficient spinel phase (LiM_2O_4) are visible (red arrows), matching those observed in the stoichiometric sample cycled at 900 °C. The inset highlights spinel-related features near the (003) peak.

To contextualize these observations within a theoretical framework, the irreversible degradation of the layered structure at elevated temperatures can be understood in terms of fundamental thermodynamic principles. The stability of the layered $LiMO_2$ (M = Ni, Mn, Co) phase is governed by the Gibbs free energy of the system ($\Delta G = \Delta H - T\Delta S$). At standard temperatures, the layered structure represents the thermodynamic minimum. However, as the temperature approaches and exceeds 900 °C, the entropic contribution ($-T\Delta S$) begins to dominate the free energy equation. This entropic driving force facilitates the release of lattice oxygen and the volatilization of lithium, often proceeding *via* the sublimation of Li_2O species. The formation of gaseous products increases the system's entropy ($\Delta S > 0$), driving ΔG increasingly negative at high temperatures and making the volatilization a thermodynamically spontaneous process. As the concentrations of lithium and oxygen vacancies exceed a critical threshold, the highly defective layered lattice becomes thermodynamically unstable. To minimize the free energy of the system, transition metals migrate through the oxygen layers, reorganizing the destabilized lattice into a spinel structure, such as LiM_2O_4. The

spinel phase is thermodynamically favoured under these lithium-deficient conditions because it can accommodate the altered stoichiometry and transition metal valence states with a lower internal energy than a highly strained, vacancy-rich layered structure.

Evaluating the electrochemical consequences of structural degradation

To validate the structural insights from the thermal analyses, the NMC 111 materials synthesized at the optimal soak temperature (800 °C) and an excessive soak temperature (900 °C) were evaluated for their electrochemical performance. The long-term stability of these materials to cycling provides a direct measure of how the structural and phase integrity established during thermal treatment of a prelithiated precursor translates into functional performance in a lithium-ion battery. The cycling data in Fig. 6 demonstrate the critical impact of the soak temperature on the electrochemical stability of these cathode materials. The materials processed at 800 °C and 900 °C exhibit a similar initial capacity of approximately 140 mAh g^{-1}. Their performance, however, diverges significantly after extended cycling up to 200 cycles.

The sample treated at 800 °C displays a markedly superior capacity retention of about 57% after 200 cycles. This stable performance is a direct consequence of the more well-ordered, crystalline layered structure achieved at this soak temperature, which minimizes irreversible cation mixing, as confirmed by the VT-XRD analyses. In contrast, the sample treated at 900 °C exhibits rapid, severe capacity degradation, retaining only 31% of its initial capacity after 200 cycles. This poor cycling stability corroborates the structural damage observed in the previous analyses. Excessive thermal energy at 900 °C induces irreversible structural degradation in the NMC cathode materials, including significant cation mixing and lithium volatilization. This lithium loss facilitates the formation of an electrochemically inferior, Li-deficient spinel phase, as evidenced by the XRD patterns of the degraded sample. The presence of this impurity phase and the overall loss of layered ordering impede Li-ion diffusion and degrade performance, consistent with the rapid capacity fade observed during cycling. This rapid capacity fade is further corroborated by the Coulombic efficiency (CE) of the cells (Fig. S6). While the sample processed at 800 °C follows a relatively smooth and predictable CE trend over 200 cycles, the sample treated at 900 °C exhibits a highly erratic and fluctuating CE, particularly in the later cycles. This unstable efficiency profile correlates with the degraded, lithium-deficient spinel phase and loss of layered ordering observed in the VT-XRD analyses.

Ultimately, the electrochemical results provide compelling evidence to support the conclusions drawn from the structural analyses. The superior cycling stability of the material prepared *via* a thermal soak at 800 °C confirms the preservation of its structural integrity, directly validating the findings from the VT-XRD analyses.

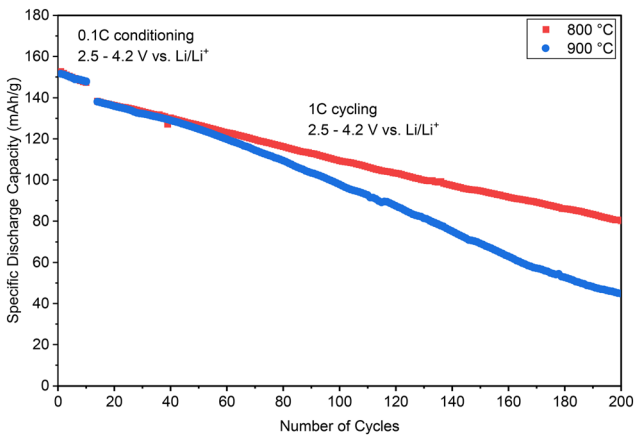

Fig. 6 Cycling performance of NMC 111 materials prepared by a synthesis that included thermal treatment with a soak at 800 °C (red) or 900 °C (blue).

Conclusions

This study provides a systematic analysis of the thermal evolution of NMC 111 during its synthesis from a prelithiated precursor. This evaluation demonstrates procedures for optimizing the preparation of NMC 111 by assessing the upper limit and soak time at elevated temperatures and their influence on the structural integrity of this cathode material. These findings demonstrate the importance of identifying and precisely controlling the synthesis temperature during the preparation of NMC 111 and other layered cathode materials. In this case, it is shown that temperatures at or above 800 °C significantly enhance the crystallinity of the product, but exceeding this threshold—particularly approaching 900 °C—induces irreversible cation mixing and the formation of a secondary phase.

Cation mixing is initiated at temperatures as low as 500 °C during the heat treatment of the prelithiated NMC 111 precursor. This mixing is, however, reversible for heat treatments up to ~800 °C. Crossing a thermal boundary between 800 and 900 °C results in permanent structural degradation of the NMC 111, as evidenced by a significant decrease in the R_1 ratio and a reduction in the quality of the layered ordering. This irreversible damage is strongly correlated with lithium loss at elevated temperatures, which facilitates the formation of spinel-like phases. The presence of these impurity phases was confirmed by powder XRD, with further validation provided by a deliberately prepared lithium-deficient control sample.

Prolonged soak durations at 800 or 900 °C were shown to improve peak sharpness and crystallinity of the sample. Further improvements in sample quality progressively diminished with extended soaking time. Notably, the sample crystallinity reached a plateau more quickly than the onset of cation mixing, underscoring the importance of balancing the soak temperature during thermal treatment with the dwell

time at this temperature. Among the conditions tested herein, a soak temperature of 800 °C offers the most favourable outcome, producing a highly crystalline layered NMC 111 structure while minimizing irreversible cation disorder and lithium volatilization.

Electrochemical testing shows that while NMC 111 materials processed at 800 °C and 900 °C have similar initial capacities (~140 mAh g^{-1}), their long-term cycling performance differs substantially. The sample treated at 800 °C retains ~57% capacity after 200 cycles due to its well-ordered layered structure. In contrast, the sample processed at 900 °C suffers severe degradation (~31% retention of its initial capacity) due to irreversible structural damage, cation mixing, and formation of Li-deficient spinel phases, confirming that 800 °C is a more optimal soak temperature for stable battery performance.

Altogether, these findings identify an ideal thermal processing window around 800 °C for the synthesis of high-quality, electrochemically stable NMC 111 from a prelithiated precursor. This work provides practical guidance for tuning the protocols to select the target temperature and the duration of the thermal treatment, which will be critical during the scale-up and manufacturing of NMC-based cathodes. The lessons of this study also offer a transferable framework for optimizing more compositionally complex systems, such as high-nickel NMC variants.

Author contributions

Jeffrey S. Ovens – conceptualization; data curation; formal analysis; investigation; methodology; project administration; visualization; writing – review & editing. Rex Chen – formal analysis; visualization; writing – original draft; writing – review & editing. Yingzi Feng – investigation; formal analysis; writing – review & editing. Majid Talebiesfandarani – resources; formal analysis; writing – review & editing. Stephen A. Campbell – conceptualization; funding acquisition; resources; formal analysis; methodology; writing – review & editing. Byron D. Gates – conceptualization; formal analysis; funding acquisition; methodology; resources; project administration; supervision; writing – review & editing.

Conflicts of interest

The authors confirm no competing financial interest.

Data availability

The data supporting this article have been included as part of the supplementary information (SI).

Supplementary information: Fig. S1 to S5, the results from thermogravimetric analyses, and Fig. S6, the Coulombic efficiency of the cycled NMC 111 cathode materials. See DOI: https://doi.org/10.1039/d6ce00043f.

Acknowledgements

This research was supported in part by the Natural Sciences and Engineering Research Council of Canada (NSERC; Grant No. RGPIN-2020-06522), a Mitacs Elevate (Grant No. IT08403) sponsored in part by Nano One Materials, and a Simon Fraser University Graduate Fellowship (R. Chen). This work made use of the 4D LABS at Simon Fraser University (SFU) and the Center for Soft Materials shared facilities supported by the Canada Foundation for Innovation (CFI), British Columbia Knowledge Development Fund (BCKDF), Western Economic Diversification Canada, and SFU.

References

1 N. Mohamed and N. K. Allam, Recent advances in the design of cathode materials for Li-ion batteries, *RSC Adv.*, 2020, **10**, 21662–21685, DOI: 10.1039/D0RA03314F.
2 J. W. Fergus, Recent developments in cathode materials for lithium ion batteries, *J. Power Sources*, 2010, **195**, 939–954, DOI: 10.1016/j.jpowsour.2009.08.089.
3 T. Chen, Y. Jin, H. Lv, A. Yang, M. Liu, B. Chen, Y. Xie and Q. Chen, Applications of Lithium-Ion Batteries in Grid-Scale Energy Storage Systems, *Trans. Tianjin Univ.*, 2020, **26**, 208–217, DOI: 10.1007/s12209-020-00236-w.
4 B. Xu, D. Qian, Z. Wang and Y. S. Meng, Recent progress in cathode materials research for advanced lithium ion batteries, *Mater. Sci. Eng., R*, 2012, **73**, 51–65, DOI: 10.1016/j.mser.2012.05.003.
5 J. C. Garcia, J. Bareño, J. Yan, G. Chen, A. Hauser, J. R. Croy and H. Iddir, Surface Structure, Morphology, and Stability of $Li(Ni_{1/3}Mn_{1/3}Co_{1/3})O_2$ Cathode Material, *J. Phys. Chem. C*, 2017, **121**, 8290–8299, DOI: 10.1021/acs.jpcc.7b00896.
6 I. Belharouak, Y.-K. Sun, J. Liu and K. Amine, $Li(Ni_{1/3}Co_{1/3}Mn_{1/3})O_2$ as a suitable cathode for high power applications, *J. Power Sources*, 2003, **123**, 247–252, DOI: 10.1016/S0378-7753(03)00529-9.
7 I. Buchberger, S. Seidlmayer, A. Pokharel, M. Piana, J. Hattendorff, P. Kudejova, R. Gilles and H. A. Gasteiger, Aging Analysis of Graphite/LiNi1/3Mn1/3Co1/3O2 Cells Using XRD, PGAA, and AC Impedance, *J. Electrochem. Soc.*, 2015, **162**, A2737, DOI: 10.1149/2.0721514jes.
8 R. Jung, M. Metzger, F. Maglia, C. Stinner and H. A. Gasteiger, Oxygen Release and Its Effect on the Cycling Stability of $LiNi_xMn_yCo_zO_2$ (NMC) Cathode Materials for Li-Ion Batteries, *J. Electrochem. Soc.*, 2017, **164**, A1361, DOI: 10.1149/2.0021707jes.
9 Z. Cui and A. Manthiram, Thermal Stability and Outgassing Behaviors of High-nickel Cathodes in Lithium-ion Batteries, *Angew. Chem., Int. Ed.*, 2023, **62**, e202307243, DOI: 10.1002/anie.202307243.
10 T. Li, X.-Z. Yuan, L. Zhang, D. Song, K. Shi and C. Bock, Degradation Mechanisms and Mitigation Strategies of Nickel-Rich NMC-Based Lithium-Ion Batteries, *Electrochem. Energy Rev.*, 2020, **3**, 43–80, DOI: 10.1007/s41918-019-00053-3.
11 E. Jo, J.-H. Park, J. Park, J. Hwang, K. Y. Chung, K.-W. Nam, S. M. Kim and W. Chang, Different thermal degradation

mechanisms: Role of aluminum in Ni-rich layered cathode materials, *Nano Energy*, 2020, **78**, 105367, DOI: 10.1016/j.nanoen.2020.105367.

12 W.-C. Chen, Y.-F. Song, C.-C. Wang, Y. Liu, D. T. Morris, P. A. Pianetta, J. C. Andrews, H.-C. Wu and N.-L. Wu, Study on the synthesis–microstructure-performance relationship of layered Li-excess nickel–manganese oxide as a Li-ion battery cathode prepared by high-temperature calcination, *J. Mater. Chem. A*, 2013, **1**, 10847–10856, DOI: 10.1039/C3TA11716B.

13 M. Malik, K. H. Chan and G. Azimi, Review on the synthesis of $LiNi_xMn_yCo_{1-x-y}O_2$ (NMC) cathodes for lithium-ion batteries, *Mater. Today Energy*, 2022, **28**, 101066, DOI: 10.1016/j.mtener.2022.101066.

14 F. Wang, P. Barai, O. Kahvecioglu, K. Z. Pupek, J. Bai and V. Srinivasan, Process design for calcination of nickel-based cathode materials by in situ characterization and multiscale modeling, *J. Mater. Res.*, 2022, **37**, 3197–3215, DOI: 10.1557/s43578-022-00678-z.

15 M. Wolfman, X. Wang, J. C. Garcia, P. Barai, J. E. Stubbs, P. J. Eng, O. Kahvecioglu, T. L. Kinnibrugh, K. E. Madsen, H. Iddir, V. Srinivasan and T. T. Fister, The Importance of Surface Oxygen for Lithiation and Morphology Evolution during Calcination of High-Nickel NMC Cathodes, *Adv. Energy Mater.*, 2022, **12**, 2102951, DOI: 10.1002/aenm.202102951.

16 J. Zheng, P. Yan, L. Estevez, C. Wang and J.-G. Zhang, Effect of calcination temperature on the electrochemical properties of nickel-rich $LiNi_{0.76}Mn_{0.14}Co_{0.10}O_2$ cathodes for lithium-ion batteries, *Nano Energy*, 2018, **49**, 538–548, DOI: 10.1016/j.nanoen.2018.04.077.

17 L. Zhang, X. Wang, T. Muta, D. Li, H. Noguchi, M. Yoshio, R. Ma, K. Takada and T. Sasaki, The effects of extra Li content, synthesis method, sintering temperature on synthesis and electrochemistry of layered $LiNi_{1/3}Mn_{1/3}Co_{1/3}O_2$, *J. Power Sources*, 2006, **162**, 629–635, DOI: 10.1016/j.jpowsour.2006.06.089.

18 X. Zhang, W. J. Jiang, A. Mauger, Qilu, F. Gendron and C. M. Julien, Minimization of the cation mixing in $Li_{1+x}(NMC)_{1-x}O_2$ as cathode material, *J. Power Sources*, 2010, **195**, 1292–1301, DOI: 10.1016/j.jpowsour.2009.09.029.

19 J. R. Dahn, U. von Sacken and C. A. Michal, Structure and electrochemistry of $Li_{1\pm y}NiO_2$ and a new Li_2NiO_2 phase with the Ni $(OH)_2$ structure, *Solid State Ionics*, 1990, **44**, 87–97, DOI: 10.1016/0167-2738(90)90049-W.

20 P. Barai, X. Wang, M. Wolfman, J. Chen, A. Gutierrez, J. C. Garcia, J. Wen, T. Kinnibrugh, T. T. Fister, H. H. Iddir and V. Srinivasan, Deciphering the morphology of transition metal carbonate cathode precursors, *J. Mater. Chem. A*, 2024, **12**, 12835–12855, DOI: 10.1039/D3TA08095A.

21 V. Charbonneau, F. Larouche, K. Amouzegar, G. Soucy and J. Veilleux, Quantification of hydroxide in co-precipitated nickel, manganese, cobalt carbonate precursor via TG-MS analyses, *Thermochim. Acta*, 2025, **750**, 180035, DOI: 10.1016/j.tca.2025.180035.

22 A. Bean Getsoian and D. Bilby, Trace Moisture Drives Lithium Volatility during Cathode Synthesis, *J. Phys. Chem. C*, 2024, **128**, 19492–19498, DOI: 10.1021/acs.jpcc.4c05055.

23 P. Barboux, J. M. Tarascon and F. K. Shokoohi, The use of acetates as precursors for the low-temperature synthesis of $LiMn_2O_4$ and $LiCoO_2$ intercalation compounds, *J. Solid State Chem.*, 1991, **94**, 185–196, DOI: 10.1016/0022-4596(91)90231-6.

24 S. Lee, C. Li and A. Manthiram, Effects of Calcination Conditions on the Structural and Electrochemical Behaviors of High-Nickel, Cobalt-Free $LiNi_{0.9}Mn_{0.1}O_2$ Cathode, *Adv. Energy Mater.*, 2024, **14**, 2400662, DOI: 10.1002/aenm.202400662.

25 L. M. Nguyen, V. H. Nguyen, D. M. N. Nguyen, M. K. Le, V. M. Tran and M. L. P. Le, Evaluating Electrochemical Properties of Layered $Na_xMn_{0.5}Co_{0.5}O_2$ Obtained at Different Calcined Temperatures, *ChemEngineering*, 2023, **7**, 33, DOI: 10.3390/chemengineering7020033.

26 M. A. Rhamdhani, E. Jak and P. C. Hayes, Basic Nickel Carbonate: Part I. Microstructure and Phase Changes during Oxidation and Reduction Processes, *Metall. Mater. Trans. B*, 2008, **39**, 218–233, DOI: 10.1007/s11663-007-9124-4.

27 Y. Li, Y. Li, Z. Zhang, X. He, J. Chen and C. Liu, Pyrolysis kinetics of manganese carbonate, *J. Therm. Anal. Calorim.*, 2022, **147**, 10801–10813, DOI: 10.1007/s10973-022-11251-5.

28 Z. Ouyang, P. Wen, Y. Chen and L. Ye, Study on thermodynamic equilibrium and character inheritance of cobalt carbonate decomposition, *Vacuum*, 2020, **179**, 109559, DOI: 10.1016/j.vacuum.2020.109559.

29 C. Zhu, G. Saito and T. Akiyama, A new $CaCO_3$-template method to synthesize nanoporous manganese oxide hollow structures and their transformation to high-performance $LiMn_2O_4$ cathodes for lithium-ion batteries, *J. Mater. Chem. A*, 2013, **1**, 7077–7082, DOI: 10.1039/C3TA11066D.

30 A. S. Amarasekara and A. B. Shrestha, Facile recovery of lithium as Li_2CO_3 or Li_2O from α-hydroxy-carboxylic acid chelates through pyrolysis and the decomposition mechanism, *J. Anal. Appl. Pyrolysis*, 2024, **179**, 106471, DOI: 10.1016/j.jaap.2024.106471.

31 X. Huang, Y. Lu, Z. Song, K. Rui, Q. Wang, T. Xiu, M. E. Badding and Z. Wen, Manipulating Li_2O atmosphere for sintering dense $Li_7La_3Zr_2O_{12}$ solid electrolyte, *Energy Storage Mater.*, 2019, **22**, 207–217, DOI: 10.1016/j.ensm.2019.01.018.

32 C. Zheng, Y. Chen, H. Dong, Y. Lu, J. Jin and Z. Wen, Dynamic lithium-compensation mechanism for densification of garnet-type $Li_7La_3Zr_2O_{12}$ electrolyte by Li_2O atmosphere buffer pair, *Nano Res.*, 2024, **17**, 6184–6191, DOI: 10.1007/s12274-024-6624-3.

33 C. L. A. Leung, M. D. Wilson, T. Connolley and C. Huang, Mapping of lithium ion concentrations in 3D structures through development of in situ correlative imaging of X-ray Compton scattering-computed tomography, *J. Synchrotron Radiat.*, 2024, **31**, 888–895, DOI: 10.1107/S1600577524003382.

34 M. H. Tahmasebi and M. N. Obrovac, New Insights into the All-Dry Synthesis of NMC622 Cathodes Using a Single-Phase Rock Salt Oxide Precursor, *ACS Omega*, 2024, **9**, 1916–1924, DOI: 10.1021/acsomega.3c08702.

35 T. E. Ashton, P. J. Baker, C. Sotelo-Vazquez, C. J. M. Footer, K. M. Kojima, T. Matsukawa, T. Kamiyama and J. A. Darr, Stoichiometrically driven disorder and local diffusion in NMC cathodes, *J. Mater. Chem. A*, 2021, **9**, 10477–10486, DOI: 10.1039/D1TA01639C.

36 T. Ungár, Microstructural parameters from X-ray diffraction peak broadening, *Scr. Mater.*, 2004, **51**, 777–781, DOI: 10.1016/j.scriptamat.2004.05.007.

37 C. F. Holder and R. E. Schaak, Tutorial on Powder X-ray Diffraction for Characterizing Nanoscale Materials, *ACS Nano*, 2019, **13**, 7359–7365, DOI: 10.1021/acsnano.9b05157.

38 Heryanto, B. Abdullah, D. Tahir and Mahdalia, Quantitative analysis of X-Ray diffraction spectra for determine structural properties and deformation energy of Al, Cu and Si, *J. Phys.: Conf. Ser.*, 2019, **1317**, 012052, DOI: 10.1088/1742-6596/1317/1/012052.

39 J.-M. Lebrun, S. K. Jha, S. J. McCormack, W. M. Kriven and R. Raj, Broadening of Diffraction Peak Widths and Temperature Nonuniformity During Flash Experiments, *J. Am. Ceram. Soc.*, 2016, **99**, 3429–3434, DOI: 10.1111/jace.14326.

40 A. Paskin, A reformulation of the temperature dependence of the Debye characteristic temperature and its effect on Debye-Waller theory, *Acta Crystallogr.*, 1957, **10**, 667–669, DOI: 10.1107/S0365110X57002303.

41 F. D. Vila, J. J. Rehr, H. H. Rossner and H. J. Krappe, Theoretical x-ray absorption Debye-Waller factors, *Phys. Rev. B: Condens. Matter Mater. Phys.*, 2007, **76**, 014301, DOI: 10.1103/PhysRevB.76.014301.

42 A. R. Genreith-Schriever, A. Alexiu, G. S. Phillips, C. S. Coates, L. A. V. Nagle-Cocco, J. D. Bocarsly, F. N. Sayed, S. E. Dutton and C. P. Grey, Jahn–Teller Distortions and Phase Transitions in $LiNiO_2$: Insights from Ab Initio Molecular Dynamics and Variable-Temperature X-ray Diffraction, *Chem. Mater.*, 2024, **36**, 2289–2303, DOI: 10.1021/acs.chemmater.3c02413.

43 M. Nurullah Ates, Q. Jia, A. Shah, A. Busnaina, S. Mukerjee and K. M. Abraham, Mitigation of Layered to Spinel Conversion of a Li-Rich Layered Metal Oxide Cathode Material for Li-Ion Batteries, *J. Electrochem. Soc.*, 2014, **161**, A290, DOI: 10.1149/2.040403jes.

44 X. Liu, C. Jiang, B. Yu, M. Wang, Y. Jin, Z. Fu, J. Chen, Z. Ma, B. Guo, Y. Huang, Z. Yang, R. Huang and X. Li, Fundamental mechanism revealed for lithium deficiencies engineering in a new spherical Li-Rich Mn-based layered $Li_{1.23}Mn_{0.46}Ni_{0.246}Co_{0.046}Al_{0.015}O_2$ cathode, *Electrochim. Acta*, 2022, **418**, 140379, DOI: 10.1016/j.electacta.2022.140379.

45 W. Hua, S. Wang, M. Knapp, S. J. Leake, A. Senyshyn, C. Richter, M. Yavuz, J. R. Binder, C. P. Grey, H. Ehrenberg, S. Indris and B. Schwarz, Structural insights into the formation and voltage degradation of lithium- and manganese-rich layered oxides, *Nat. Commun.*, 2019, **10**, 5365, DOI: 10.1038/s41467-019-13240-z.

46 P. Tammawat, T. Sesuk, P. Eiamlamai, P. Limthongkul and N. Kunanusont, Direct regeneration of spent $LiNi_{0.8}Mn_{0.1}Co_{0.1}O_2$ via thermal treatment and solid-state reaction: A closed-loop and versatile direct recycling process for Li-ion batteries degraded under various conditions, *J. Power Sources*, 2025, **641**, 236827, DOI: 10.1016/j.jpowsour.2025.236827.

47 T.-P. Gao, K. W. Wong, K. Y. Fung, W. Zhang and K. M. Ng, A rational three-step calcination strategy for synthesizing high-quality $LiNi_{0.5}Mn_{0.3}Co_{0.2}O_2$ cathode materials: The key role of suppressing Li_2O formation, *Electrochim. Acta*, 2018, **288**, 153–164, DOI: 10.1016/j.electacta.2018.09.012.

48 T. Wang, K. Ren, M. He, W. Dong, W. Xiao, H. Pan, J. Yang, Y. Yang, P. Liu, Z. Cao, X. Ma and H. Wang, Synthesis and Manipulation of Single-Crystalline Lithium Nickel Manganese Cobalt Oxide Cathodes: A Review of Growth Mechanism, *Front. Chem.*, 2020, **8**, 747, DOI: 10.3389/fchem.2020.00747.